

# Photoconductance and inverse photoconductance in films of functionalized metal nanoparticles

Hideyuki Nakanishi<sup>1,2</sup>, Kyle J. M. Bishop<sup>2</sup>, Bartłomiej Kowalczyk<sup>1,2</sup>, Abraham Nitzan<sup>1,3</sup>, Emily A. Weiss<sup>1</sup>, Konstantin V. Tretiakov<sup>2</sup>, Mario M. Apodaca<sup>1</sup>, Rafal Klajn<sup>2</sup>, J. Fraser Stoddart<sup>1</sup> & Bartosz A. Grzybowski<sup>1,2</sup>

In traditional photoconductors<sup>1–3</sup>, the impinging light generates mobile charge carriers in the valence and/or conduction bands, causing the material's conductivity to increase<sup>4</sup>. Such positive photoconductance is observed in both bulk and nanostructured<sup>5,6</sup> photoconductors. Here we describe a class of nanoparticle-based materials whose conductivity can either increase or decrease on irradiation with visible light of wavelengths close to the particles' surface plasmon resonance. The remarkable feature of these plasmonic materials is that the sign of the conductivity change and the nature of the electron transport between the nanoparticles depend on the molecules comprising the self-assembled monolayers (SAMs)<sup>7,8</sup> stabilizing the nanoparticles. For SAMs made of electrically neutral (polar and non-polar) molecules, conductivity increases on irradiation. If, however, the SAMs contain electrically charged (either negatively or positively) groups, conductivity decreases. The optical and electrical characteristics of these previously undescribed inverse photoconductors can be engineered flexibly by adjusting the material properties of the nanoparticles and of the coating SAMs. In particular, in films comprising mixtures of different nanoparticles or nanoparticles coated with mixed SAMs, the overall photoconductance is a weighted average of the changes induced by the individual components. These and other observations can be rationalized in terms of light-induced creation of mobile charge carriers whose transport through the charged SAMs is inhibited by carrier trapping in transient polaron-like states<sup>9,10</sup>. The nanoparticle-based photoconductors we describe could have uses in chemical sensors and/or in conjunction with flexible substrates.

We used gold and silver nanoparticles (diameter  $5.6 \pm 0.8$  nm, with surface plasmon resonance (SPR) maxima in solution of respectively  $\lambda_{\max}^{\text{Au}} \approx 520$  nm and  $\lambda_{\max}^{\text{Ag}} \approx 420$  nm) synthesized as described before<sup>11–13</sup>; these were stabilized by monocomponent or mixed SAMs of alkane thiols (Fig. 1a) abbreviated as C<sub>3</sub>OH, C<sub>6</sub>OH, C<sub>11</sub>OH, C<sub>10</sub>COOH, C<sub>11</sub>NMe<sub>3</sub><sup>+</sup>, C<sub>6</sub>, PhOH and PhCOOH. The suspensions of the nanoparticles were drop-cast onto a glass or Teflon substrate, and the solvent was evaporated under vacuum to give nanoparticle films of thickness ( $h$ ) 120–300 nm (determined by profilometry for each sample), and characterized by SPR bands red-shifted (by ~50–60 nm) and broadened owing to nanoparticle aggregation<sup>13,14</sup> (Fig. 1c). Next, Pd/Au electrodes (width  $w = 5$  mm, separated by a gap of  $L = 50$   $\mu\text{m}$ ; Fig. 1b) were sputtered onto the films, which were then dried under high vacuum for at least one week to remove traces of solvent and water. The samples were placed in a custom-made, hermetically sealed Faraday cage under inert atmosphere and in the presence of phosphorus pentoxide, a dehydrating agent. The electrodes were connected to a Keithley 6517 electrometer, a white-light LED (light-emitting diode) was placed above the film,

and optical bandpass filters were used to select the desired wavelength of light. Unless otherwise noted, the temperature during all experiments was kept constant to within 0.02 °C (for further experimental details, see Supplementary Information section 1).

In the absence of irradiation, both Au and Ag films exhibit ohmic current density–applied field ( $j$ – $E$ ) characteristics in the field intensity range from 100 V m<sup>–1</sup> (corresponding to 0.005 V across the system and sub-picoamp currents at the sensitivity limit of the electrometer) to 20 kV m<sup>–1</sup> (higher fields cause irreversible changes in the nanoparticle films and coalescence of the neighbouring nanoparticles).

Irradiation with visible light alters the currents through the nanostructured films (Fig. 2). We note that the signs of the observed

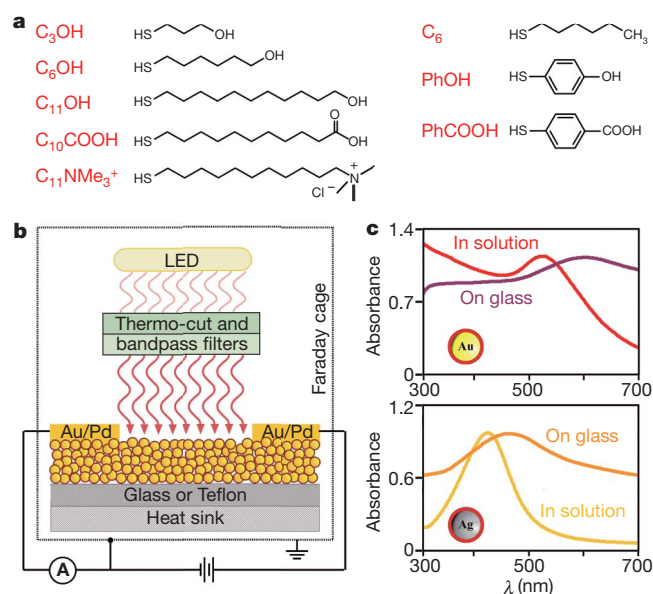


**Figure 1 | Functionalized nanoparticles for photoconductive films.**

**a**, Structures of alkane thiols used to form SAMs on gold and/or silver nanoparticles. **b**, Diagram of the experimental set-up (not to scale). The thickness of the nanoparticle layer is ~120–300 nm. Thinner layers give currents of magnitude comparable to the external/instrument noise. **c**, Ultraviolet/visible spectra of Au/C<sub>6</sub>OH (top) and Ag/C<sub>6</sub>OH (bottom) nanoparticles in solution and when cast onto glass films. Note that owing to aggregation of the nanoparticles<sup>12,13</sup>, the spectra of the particles in the films are broadened and red-shifted compared to those of free particles in solution. The degree of this spectral shift increases with decreasing thickness of SAMs separating the metal cores of the nanoparticles (for example,  $\lambda_{\max}^{\text{Au}} \approx 580$  nm for Au/C<sub>6</sub>OH films but  $\lambda_{\max}^{\text{Au}} \approx 770$  nm for Au/C<sub>3</sub>OH films).

<sup>1</sup>Department of Chemistry, <sup>2</sup>Department of Chemical and Biological Engineering, Northwestern University, 2145 Sheridan Road, Evanston, Illinois 60208, USA. <sup>3</sup>School of Chemistry, Tel Aviv University, Tel Aviv, Israel.

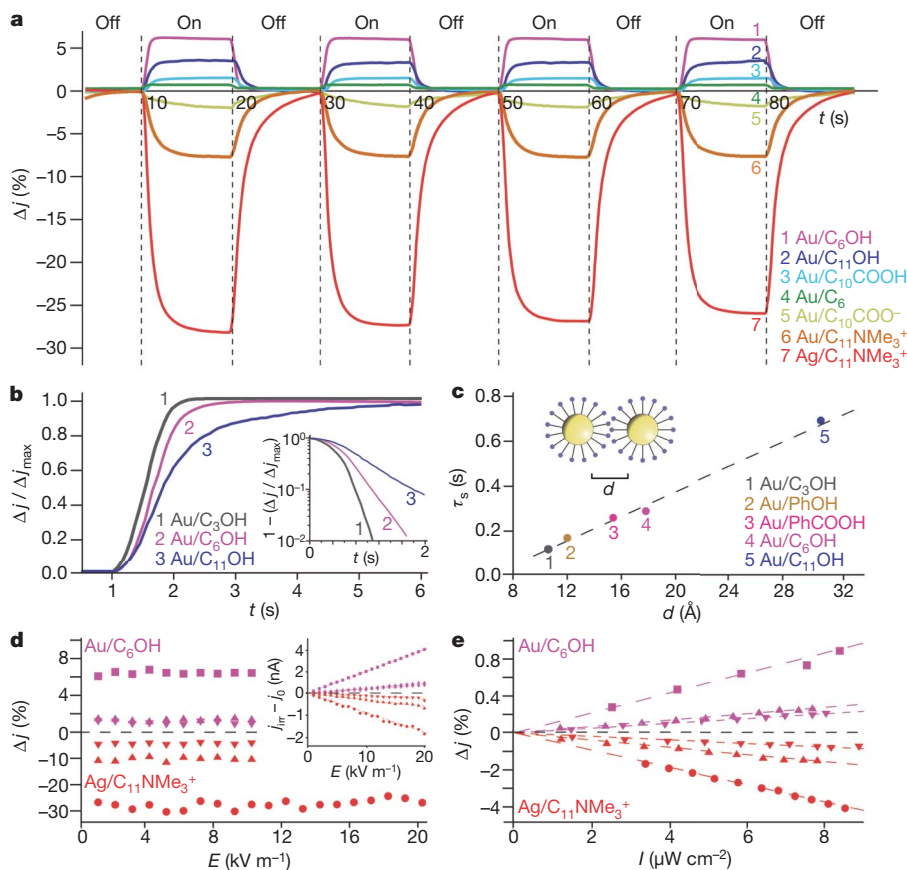


**Figure 2 | Photoconductance and inverse photoconductance of irradiated nanoparticle films.** **a**, Change in current density on irradiation,  $\Delta j$ , for various types of nanoparticle films irradiated periodically with white LED light. Key specifies metal cores and coating thiols (Fig. 1a). Control experiments with thin films of thermally evaporated Au or Ag show no conductivity changes on irradiation. **b**, Dependence of  $\Delta j$  on time  $t$  (immediately after the irradiation commences) for a series of uncharged thiols differing only in chain length. Inset, linear regions in the semi-log plot correspond to an exponential  $\Delta j(t)$  dependence; slopes equal the inverse of  $\tau_s$ . **c**,  $\tau_s$  decreases approximately linearly with decreasing thickness,  $d$ , of SAMs separating nanoparticle metal cores;  $d$  was estimated from molecular modelling and, independently, from TEM images of the films (methods agreed to within 15%). Errors in the times are of the order of a few per cent

changes depend on the chemical nature of the thiols coating the nanoparticles but not on the nature of the particles' metal cores. Figure 2a shows typical variations in the relative current density,  $\Delta j \equiv (j_{\text{irr}} - j_0)/j_0$  ( $j_0$  and  $j_{\text{irr}}$  indicate current density in the respective absence and presence of irradiation), recorded for different types of nanoparticle films (all at  $E = 20 \text{ kV m}^{-1}$  and for nanoparticles coated with monocomponent SAMs) periodically exposed to white LED light of intensity  $I_{\text{white}} = 60 \mu\text{W cm}^{-2}$ . When the thiols are electrically neutral, current density increases on irradiation,  $\Delta j > 0$ . When, however, the thiols contain electrically charged groups,  $\Delta j < 0$ . Decreasing current densities are observed in films composed of either positively charged nanoparticles (coating thiol  $\text{C}_{11}\text{NMe}_3^+$ ) or negatively charged nanoparticles (deprotonated thiol  $\text{C}_{10}\text{COO}^-$ ). Interestingly, films comprising nanoparticles stabilized with protonated thiols  $\text{C}_{10}\text{COOH}$  exhibit positive  $\Delta j$  changes (compare curves 3 and 5 in Fig. 2a).

When light is switched on or off,  $\Delta j(t)$  depends on time  $t$  approximately exponentially,  $\Delta j(t) \propto (-t/\tau_s)$ , where  $\tau_s$  denotes a characteristic 'switching' time, which is the same for 'on' and 'off' exponents, does not depend on the intensity of light, and is of the order of hundreds of milliseconds. For a given terminal functionality of the thiol molecules comprising the SAMs, the switching times increase

(~7%) based on measurements of five cycles of irradiation for at least three independent samples. **d**, Irrespective of  $E$ , and for a given value of  $I$  (here,  $60 \mu\text{W cm}^{-2}$ ), the changes in photocurrent  $|\Delta j(\lambda)|_I$  are maximal when  $\lambda$  is close to the SPR maximum of the nanoparticles in the film. Violet symbols, Au/ $\text{C}_6\text{OH}$  films (maximal  $|\Delta j(\lambda)|_I$  at around  $\lambda_{\text{max}}^{\text{Au}} = 580 \text{ nm}$ ); red symbols, Ag/ $\text{C}_{11}\text{NMe}_3^+$  films (maximal  $|\Delta j(\lambda)|_I$  at  $\lambda_{\text{max}}^{\text{Ag}} = 470 \text{ nm}$ ); circles, 370–440 nm; squares, 410–500 nm; inverted triangles, 640–780 nm. Inset, absolute values of current density illustrating linear dependence of  $j_{\text{irr}} - j_0$  on  $E$ . **e**, For constant  $E$  (here,  $20 \text{ kV m}^{-1}$ ) and for different wavelengths,  $\lambda$ , relative current densities scale linearly with the intensity of irradiating light,  $\Delta j(I) \propto I$ . Symbols and wavelength ranges as in **d**. For different material samples (>5 for each condition/material tested), the values of  $\tau_s$ , and  $\Delta j$  in **c–e** agree to within less than 6%.

approximately linearly with increasing chain length (Fig. 2b and c). For identical SAMs, the switching times increase with decreasing nanoparticle size (for example,  $\tau_s \approx 0.29 \text{ s}$  for Au/ $\text{C}_6\text{OH}$  with metal core diameter 5.6 nm versus  $\tau_s \approx 0.18 \text{ s}$  for 10.0-nm Au/ $\text{C}_6\text{OH}$  particles). We note that in all cases the values of  $\tau_s$  are not related to the intrinsic current 'response' times of the measuring device (<1 ms) accompanying the step-wise change in the applied field.

A second set of observations relates the magnitudes of the relative current changes,  $|\Delta j|$ , to the field strength,  $E$ , the wavelength,  $\lambda$ , and the intensity,  $I$ , of the irradiating light. For all films studied and all values of  $\lambda$ , we find that both the 'dark' current and the light-induced change are linear in  $E$ , such that the relative light-induced change  $|\Delta j(E)|_{I,\lambda}$  is independent of  $E$  (Fig. 2d). Furthermore, at constant  $\lambda$ ,  $|\Delta j(I)|_{E,\lambda}$  is linear in the light intensity  $I$  (up to about tens of  $\mu\text{W cm}^{-2}$ ; for higher intensities, photocurrent effects are masked by increasing temperature of the film). Figure 2e illustrates this effect for Au/ $\text{C}_6\text{OH}$  and Ag/ $\text{C}_{11}\text{NMe}_3^+$  films irradiated with light of intensity up to  $I = 8 \mu\text{W cm}^{-2}$ . The corresponding slope depends on the nature of the nanoparticles/SAM and on the wavelength  $\lambda$ . Finally, for all values of  $E$  and  $I$ ,  $|\Delta j(\lambda)|_{E,I}$  is maximal when  $\lambda$  coincides with the SPR of the aggregated nanoparticles' metal cores. Thus, for Au- and Ag-based films,  $|\Delta j|$  is maximal when the wavelength is close to  $\lambda_{\text{max}}^{\text{Au}} = 580 \text{ nm}$

and  $\lambda_{\text{max}}^{\text{Ag}} = 470$  nm, respectively (Fig. 2d and e). For films comprising both Au and Ag particles, the superposition of the two SPR peaks results in maximal current changes over a wider range of wavelengths,  $\lambda \approx 400\text{--}650$  nm. In all of the above experiments, the largest current density change for uncharged thiols is  $\sim 6\%$  for Au/C<sub>6</sub>OH films. For charged thiols, changes as large as  $-27\%$  are observed for films composed of Ag/C<sub>11</sub>NMe<sub>3</sub><sup>+</sup> nanoparticles (compare Fig. 2a).

Both positive and inverse photoconductance can be explained qualitatively by a model (Supplementary Information sections 2, 3) in which the nanoparticle array is characterized by a density  $N_t$  of discrete ‘trap sites’ of which  $n_t$  are filled at thermal equilibrium. Physically, we suggest that these traps are of two types: (1) sites on

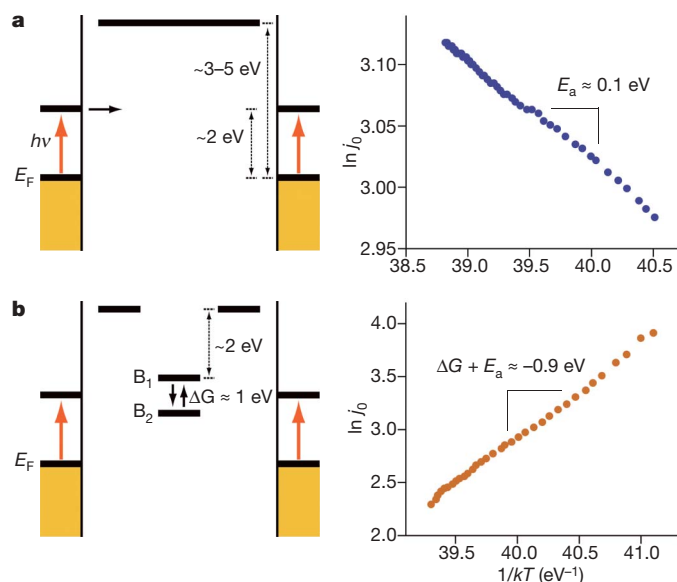


**Figure 3 | Energy diagrams and temperature dependence of responses.**

**a**, Left panel: qualitative electronic structure diagram for nanoparticles capped with uncharged ligands. Yellow bars, nanoparticles’ metal cores characterized by Fermi energies,  $E_F$ , which in the absence of irradiation define an approximate border between occupied and unoccupied states. On irradiation, electrons are promoted into excited metal states,  $\sim 2$  eV above<sup>9,10,21</sup>  $E_F$ . Molecular levels of the non-polar alkane thiols lie  $\sim 3\text{--}5$  eV above<sup>15,20</sup>  $E_F$ . Right panel: current through a film of Au/C<sub>11</sub>OH nanoparticles as a function of inverse temperature (differences in slopes recorded for different material samples are within 4% of the average). Because  $\ln(j_0) \approx -E_a/k_B T + \text{constant}$  (ref. 26), the slope ( $E_a$ ) corresponds to the amount of energy that the environment contributes to the charge transport process (probably a mixture of thermally activated hopping and temperature-independent tunnelling). **b**, For nanoparticles capped with charged ligands, the scenario presented in **a** is augmented by the presence of polaron-like states within the organic layer separating the nanoparticles. The existence of these states is supported by temperature dependent current measurements (right; Au/C<sub>11</sub>NMe<sub>3</sub><sup>+</sup>, error in the slope  $< 4\%$ ) showing that charge transport through arrays of charged nanoparticles is negatively activated (increasing the temperature decreases the current for a given applied voltage). Negative activation is common in charge transport systems<sup>26</sup> where an equilibrium exists between two conformational states of a donor-bridge-acceptor complex. Here, the molecular orbitals comprising the charged moieties (that is, the bridge) are characterized by two conformations (left), one of which ( $B_1$ ) is more favourable for electron transfer than the other ( $B_2$ ). Negative activation occurs when raising the temperature pushes the conformational equilibrium towards the unfavourable geometry ( $B_2$ ) (Supplementary Information section 2). The observed activation barrier,  $E_a^{\text{obs}} = E_a + \Delta G \approx -0.9$  eV, can be used to estimate the difference in free energy,  $\Delta G$ , between the two bridge conformations—here,  $\Delta G \approx -1$  eV. Also, the energy of bridge states corresponding to the polar groups before polaronic reorganization is  $\sim 2$  eV below those of the alkyl chains (refs 27–29; Supplementary Information section 2). Thus, in the presence of light irradiation, the lower energy bridge state ( $B_2$ ) can act as a trap for charge carriers, resulting in a negative photocurrent (main text).

the nanoparticle ‘cores’, and (2) sites on the organic ligands. The former arise because the Fermi energy of the nanoparticles is several eV below<sup>15</sup> that of the alkyl chains separating the particles. Therefore, each nanoparticle can accommodate a certain number of electrons depending on its charging energy, which in turn depends on the nanoparticle radius and capacitance<sup>16,17</sup>. In reality, charge carriers ‘trapped’ on the cores are delocalized over the particles’ surface; however, for simplicity we treat each core as a collection of discrete trap sites, each of which can accommodate a single charge carrier. Additionally, the organic ligands separating the nanoparticle cores may also act as traps if (as in the case of charged thiols discussed below) their conduction orbitals are of lower energy than the plasmon state of the nanoparticles. Within the framework of this simple but widely used trapping model<sup>18,19</sup>, the effective equilibrium between free and trapped carriers ( $n$  and  $n_t$ , respectively) is given by:

$$\frac{n[N_t - n_t]}{n_t} = K \quad (1)$$

where  $K$  is an effective equilibrium constant characterizing the density of free and trapped carriers at the steady state (Supplementary Information section 3.4). In this way, the density of traps determines the density of free charge carriers,  $n$ , and thereby the conduction current,  $j = -e\mu nE$ , where  $e$  is the fundamental charge, and  $\mu$  is the mobility of the charge carrier in the nanoparticle medium.

For arrays of nanoparticles capped with uncharged ligands, the only trap sites are those on the nanoparticle cores (see Fig. 3a), and electrons tunnel from nanoparticle to nanoparticle through a large barrier imposed by the insulating organic SAM. This barrier is  $3\text{--}5$  eV (refs 15, 20) relative to the Fermi energy of gold ( $-5.1$  eV; ref. 15) or silver ( $-4.3$  eV; ref. 15). Starting from the steady-state current in the dark, photoexcitation at or near the plasmon resonance of the nanoparticles (Fig. 2d, e) promotes electrons from the valence band to the conduction band of the nanoparticles. Subsequently, the photoexcited electrons ‘fill’ available trap sites present on the nanoparticles, thereby reducing the effective density of these sites by  $\Delta N_t = N_t^{\text{irr}} - N_t < 0$ . Through the effective equilibrium relation (1), the decrease in  $N_t$  acts to increase the density of free carriers,  $n$ , and produces a positive  $\Delta j$  in the uncharged-SAM systems.

For arrays of nanoparticles capped with charged SAMs, the traps on the nanoparticle cores are supplemented by trap sites on the organic ligands (see Fig. 3b). These additional traps probably arise due to the formation of polaron-like states via the so-called bootstrap mechanism, whereby electron localization occurs through the reorganization of the nuclear environment of the ionic moieties in the presence of an electron<sup>9,10,21</sup>. The degree of energetic stabilization of these polaronic traps via nuclear reorganization was estimated experimentally at  $\sim 1.0$  eV from the temperature dependence of the conduction current (Fig. 3b right, and Supplementary Information section 2). In the dark, the energy of these states is expected to lie above the Fermi energy of the nanoparticles, and the organic ligands do not act as trap sites but rather as part of the tunnelling barrier (Fig. 3b left). On irradiation, however, excitation at the plasmon resonance of the nanoparticles promotes charge carriers to an injection energy that is  $\sim 2$  eV above their injection energy in the dark<sup>9,10,21</sup>. Relative to this excited state, the charged ligands become effective trap sites on irradiation, thereby increasing the density of traps  $\Delta N_t > 0$  (see Supplementary Information section 3.4 for an alternative but ultimately equivalent kinetic interpretation). Consequently, the density of free carriers,  $n$ , decreases in accordance with equation (1), and the current decreases to give a negative  $\Delta j$  in the charged systems.

We note that the formation of polaron-like traps cannot be affected by the electric field produced by the oscillating electron density of the plasmon on the nanoparticles (Supplementary Information section 4). Conduction electrons on the nanoparticles excited at or near the plasmon resonance oscillate at optical frequencies ( $\sim 10^{14}$  Hz) and cannot couple to molecular motions/structural rearrangement within the organic SAMs. Furthermore, the d.c. fields produced by

these oscillations are, for the particle sizes used here, vanishingly small, and so cannot align dipoles within charged SAMs<sup>22,23</sup>.

An interesting manifestation of the two trapping scenarios is seen when the films contain both uncharged and charged ligands. Figure 4a plots the results of a series of experiments with films comprising (1) binary mixtures of charged and uncharged nanoparticles (here, Au/C<sub>11</sub>NMe<sub>3</sub><sup>+</sup> and Au/C<sub>11</sub>OH; blue squares) and (2) nanoparticles coated with mixed SAMs<sup>24</sup> of charged and uncharged thiols (C<sub>11</sub>NMe<sub>3</sub><sup>+</sup> and C<sub>11</sub>OH; yellow circles). For both types of system, the overall relative current changes can be expressed as a linear combination of the current changes of monocomponent films,  $\Delta j = \chi_{\text{OH}} \Delta j_{\text{OH}} + \chi_{\text{NMe}_3^+} \Delta j_{\text{NMe}_3^+}$ , where  $\chi_{\text{OH}}$  and  $\chi_{\text{NMe}_3^+} = 1 - \chi_{\text{OH}}$  are the fractions of either nanoparticles of each type in the film or of different thiols on the nanoparticle surfaces. These linear dependences imply that the effects of polaronic-like centres on carrier trapping are additive, such that the number of trapping sites introduced on irradiation increases linearly with the number of charged moieties in the material (Supplementary Information section 3.3.vi). Interestingly, at a particular ratio  $\chi_{\text{OH}} \approx 0.6$ , the increase in the number of mobile carriers created by photoexcitation is exactly offset by the increase in the number of traps due to charged thiols, such that the effective number of trapping sites remains unchanged on irradiation and the photocurrent is identical to the dark current,  $\Delta j = 0$ .

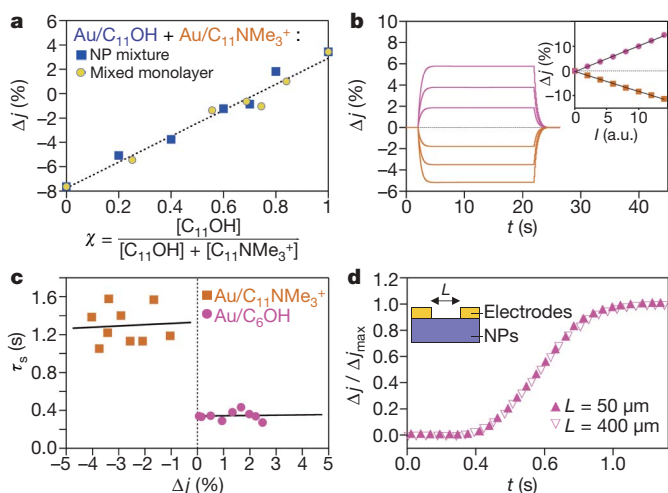


**Figure 4 | Conductance of mixed films and theoretical predictions.** **a**, Typical linear dependence of  $\Delta j$  on the composition  $\chi$  of the nanoparticle films. Blue squares, films composed of Au/C<sub>11</sub>OH and Au/C<sub>11</sub>NMe<sub>3</sub><sup>+</sup> nanoparticles (NPs). Yellow circles, films comprising Au nanoparticles coated with mixed SAMs of C<sub>11</sub>OH and C<sub>11</sub>NMe<sub>3</sub><sup>+</sup> thiols. Correlation coefficients:  $r^2 = 0.982$  for nanoparticle mixtures,  $r^2 = 0.976$  for mixed-SAM nanoparticles,  $r^2 = 0.962$  for all data points; errors based on the analysis of at least seven samples per condition are less than  $\sim 10\%$  of the averages shown. Similar linear trends are observed for other thiol pairs studied. Dashed line (fit) indicates that this linear trend is also predicted by the theoretical model (see main text). **b**, Positive and negative photocurrent response as calculated by charge transport simulations (Supplementary Information section 3). The current change on irradiation (or ceasing of irradiation) is well approximated by an exponential saturation to the new steady-state current with a switching time characteristic of the trapping kinetics (here,  $\tau_s = 0.5$  s). Inset, the magnitude of the photoresponse is linearly proportional to the light intensity. **c**, Experimentally recorded  $\tau_s$  as a function of  $\Delta j$  for Au/C<sub>11</sub>NMe<sub>3</sub><sup>+</sup> and Au/C<sub>6</sub>OH nanoparticle arrays using light irradiation of different intensities. Solid lines, theoretical fits from the charge transport model, illustrating that  $\tau_s$  is largely independent of the magnitude of  $\Delta j$  but depends on the nature of the ligands (here  $\tau_s \approx 1.3$  s for Au/C<sub>11</sub>NMe<sub>3</sub><sup>+</sup> and  $\tau_s \approx 0.34$  s for Au/C<sub>6</sub>OH). **d**, Photocurrent response for Au/C<sub>6</sub>OH nanoparticles for two different electrode separations,  $L = 50$   $\mu\text{m}$  and  $400$   $\mu\text{m}$ . The switching time does not depend on  $L$  (in agreement with theoretical prediction) but only on the nature of the 'trap sites' within the nanoparticles and, in the case of charge ligands, within the organic layer.

To gain further insight into the response of the material to light irradiation, it is necessary to account for the kinetic processes of trapping or trap-emptying. Starting from the charge transport equations (Supplementary Information section 3), the positive and negative changes in the current density on photoexcitation can be related to the changes in the total number of trap sites (from  $N_t$  in the dark to  $N'_t$  on irradiation) and the concomitant changes in the number of free charge carriers (from  $n$  to  $n'$ ) subject to equation (1). It can be shown that in the absence of significant space charge injection<sup>18,19</sup>, the transport equations can be simplified to give the following equation relating changes in  $n$  to the trapping kinetics:

$$\frac{dn}{dt} = -\frac{dn_t}{dt} = k[-n(N'_t - n_t) + Kn_t] \quad (2)$$

where  $k$  is a rate constant for trapping. In the limit of  $N_t \gg n_t$  this equation is linear and predicts the exponential saturation of  $n$  and  $n_t$  to their new steady-state values: importantly, as  $j \propto n$ , the model reproduces the exponential response of the system when light is switched on or off and also the linear dependence of  $j$  on the light intensity (Fig. 4b). Furthermore,  $\tau_s \approx 1/kN_t$  (Supplementary Information section 3), so that the switching timescale observed in experiments (0.1–1 s) is equivalent to that associated with charge trapping. This timescale is commensurate with but slightly faster than the 10–100 s trapping times previously found for charge retention within gold nanoparticle transistors<sup>25</sup>. The model also correctly predicts that for a given type of SAM, the switching time depends neither on  $\Delta j$  (Fig. 4c) nor on the width of the gap between the electrodes (Fig. 4d). Finally, the model reproduces the linear dependence of  $\tau_s$  on the SAM thickness (compare Fig. 2c) and its decrease

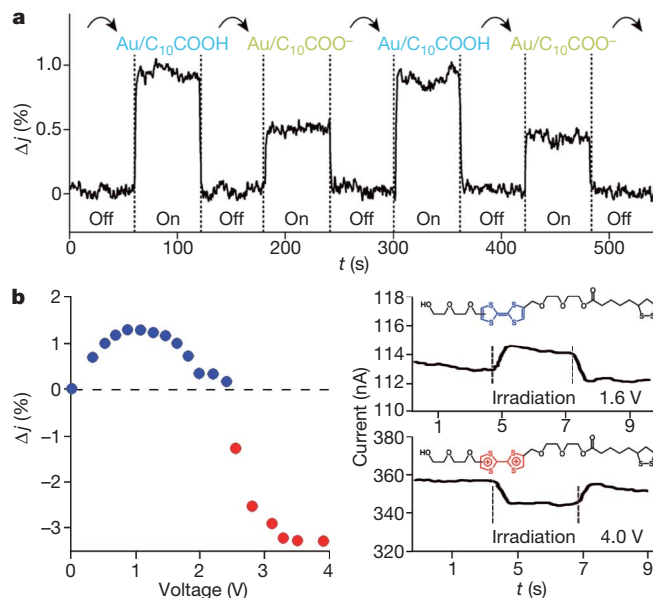


**Figure 5 | Modulation and 'switching' of photoconductance.** **a**, Exposure of a film of Au nanoparticles coated with COOH thiols to the vapours of ammonium hydroxide causes partial deprotonation of carboxylic acid groups and decreases the photocurrent; exposure to vapours of hydrochloric acid re-protonates these groups causing the photocurrent to increase. As the current does not switch to negative values observed for nanoparticles coated with fully deprotonated thiols (Fig. 2a), the deprotonation is probably only partial and/or limited by penetration of the film by the vapours' molecules. Note that this experiment is performed in the presence of humidity, and the photoconductance effect is still observed. In fact, we verified that exposure of the film to neutral water vapour (relative humidity RH < 30%) does not alter photoconductance. **b**, Switching from positive to negative (inverse) photoconductance in a film of Au nanoparticles coated with ligands terminated in tetrathiafulvalene (TTF; structural formulae shown). The effect can be attributed to the TTF  $\rightarrow$  TTF<sup>2+</sup> oxidation (blue, neutral TTF; red, TTF dication) previously reported to occur at  $\sim 2$  V (ref. 30).

with increasing nanoparticle size (because as the volume fraction of gold within the film decreases, the density of traps within the array decreases).

We have described a class of nanostructured materials that exhibit photoconductance as well as previously undescribed inverse photoconductance. From a fundamental perspective, the present work provides new insights into electron transport in heterogeneous nanostructured media in which photoexcitation and trapping of charge carriers can be spatially separated between metallic nanoparticle and insulating SAM domains. Incorporation of molecules that can be interconverted between charged and uncharged forms could enable external control of the degree of photoconductance (for example, by chemical means, Fig. 5a) or even switching between normal and inverse photoconductance modes (for example, by the applied bias, Fig. 5b).

Received 9 December 2008; accepted 11 May 2009.

- Adam, D. *et al.* Fast photoconduction in the highly ordered columnar phase of discotic liquid-crystal. *Nature* **371**, 141–143 (1994).
- Sze, S. M. *Physics of Semiconductor Devices* (Wiley & Sons, 1981).
- Yu, G., Gao, J., Hummelen, J. C., Wudl, F. & Heeger, A. J. Polymer photovoltaic cells — enhanced efficiencies via a network of internal donor-acceptor heterojunctions. *Science* **270**, 1789–1791 (1995).
- Joshi, N. V. *Photoconductivity: Art, Science and Technology* (Marcel Dekker, 1990).
- Han, S. *et al.* Photoconduction studies on GaN nanowire transistors under UV and polarized UV illumination. *Chem. Phys. Lett.* **389**, 176–180 (2004).
- Hayden, O., Agarwal, R. & Lieber, C. M. Nanoscale avalanche photodiodes for highly sensitive and spatially resolved photon detection. *Nature Mater.* **5**, 352–356 (2006).
- Love, J. C., Estroff, L. A., Kriebel, J. K., Nuzzo, R. G. & Whitesides, G. M. Self-assembled monolayers of thiolates on metals as a form of nanotechnology. *Chem. Rev.* **105**, 1103–1169 (2005).
- Witt, D., Klajn, R., Barski, P. & Grzybowski, B. A. Applications properties and synthesis of omega-functionalized n-alkanethiols and disulfides — the building blocks of self-assembled monolayers. *Curr. Org. Chem.* **8**, 1763–1797 (2004).
- Galperin, M., Ratner, M. A. & Nitzan, A. Hysteresis, switching, and negative differential resistance in molecular junctions: a polaron model. *Nano Lett.* **5**, 125–130 (2005).
- Kuznetsov, A. M. Negative differential resistance and switching behavior of redox-mediated tunnel contact. *J. Chem. Phys.* **127**, 084710 (2007).
- Kalsin, A. M. *et al.* Electrostatic self-assembly of binary nanoparticle crystals with a diamond-like lattice. *Science* **312**, 420–424 (2006).
- Kalsin, A. M., Kowalczyk, B., Smoukov, S. K., Klajn, R. & Grzybowski, B. A. Ionic-like behavior of oppositely charged nanoparticles. *J. Am. Chem. Soc.* **128**, 15046–15047 (2006).
- Kalsin, A. M. *et al.* Electrostatic aggregation and formation of core-shell suprastructures in binary mixtures of charged metal nanoparticles. *Nano Lett.* **6**, 1896–1903 (2006).
- Pinchuk, A. O., Kalsin, A. M., Kowalczyk, B., Schatz, G. C. & Grzybowski, B. A. Modeling of electrodynamic interactions between metal nanoparticles aggregated by electrostatic interactions into closely-packed clusters. *J. Phys. Chem. C* **111**, 11816–11822 (2007).
- Engelkes, V. B., Beebe, J. M. & Frisbie, C. D. Length-dependent transport in molecular junctions based on SAMs of alkanethiols and alkanedithiols: effect of metal work function and applied bias on tunneling efficiency and contact resistance. *J. Am. Chem. Soc.* **126**, 14287–14296 (2004).
- Bozano, L. D. *et al.* Organic materials and thin-film structures for cross-point memory cells based on trapping in metallic nanoparticles. *Adv. Funct. Mater.* **15**, 1933–1939 (2005).
- Lee, J. S. *et al.* Layer-by-layer assembled charge-trap memory devices with adjustable electronic properties. *Nature Nanotechnol.* **2**, 790–795 (2007).
- Lampert, M. A. Simplified theory of space-charge-limited currents in an insulator with traps. *Phys. Rev.* **103**, 1648–1656 (1956).
- Many, A. & Rakavy, G. Theory of transient space-charge-limited currents in solids in presence of trapping. *Phys. Rev.* **126**, 1980–1988 (1962).
- Lee, T. *et al.* Comparison of electronic transport characterization methods for alkanethiol self-assembled monolayers. *J. Phys. Chem. B* **108**, 8742–8750 (2004).
- Nitzan, A. *Chemical Dynamics in Condensed Phases* (Oxford Univ. Press, 2006).
- Willets, K. A. & Van Duyne, R. P. Localized surface plasmon resonance spectroscopy and sensing. *Annu. Rev. Phys. Chem.* **58**, 267–297 (2007).
- Zou, S. L. & Schatz, G. C. in *Surface-Enhanced Raman Scattering: Physics and Applications* (eds Kneipp, K., Moskovits, M. & Kneipp, H.) 67–85 (Topics in Applied Physics, Vol. 103, Springer, 2006).
- Kalsin, A. M., Kowalczyk, B., Wesson, P., Paszewski, M. & Grzybowski, B. A. Studying the thermodynamics of surface reactions on nanoparticles by electrostatic titrations. *J. Am. Chem. Soc.* **129**, 6664–6665 (2007).
- Novembre, C., Guerin, D., Lmimouni, K., Gamrat, C. & Vuillaume, D. Gold nanoparticle-pentacene memory transistors. *Appl. Phys. Lett.* **92**, 103314 (2008).
- Weiss, E. A. *et al.* Conformationally gated switching between superexchange and hopping within oligo-p-phenylene-based molecular wires. *J. Am. Chem. Soc.* **127**, 11842–11850 (2005).
- Jortner, J. & Noyes, R. M. Some thermodynamic properties of the hydrated electron. *J. Phys. Chem.* **70**, 770–774 (1966).
- Schnitker, J. & Rossky, P. J. Quantum simulation study of the hydrated electron. *J. Chem. Phys.* **86**, 3471–3485 (1987).
- Zhan, C. G. & Dixon, D. A. The nature and absolute hydration free energy of the solvated electron in water. *J. Phys. Chem. B* **107**, 4403–4417 (2003).
- Nguyen, T. D. *et al.* A reversible molecular valve. *Proc. Natl Acad. Sci. USA* **102**, 10029–10034 (2005).

**Supplementary Information** is linked to the online version of the paper at [www.nature.com/nature](http://www.nature.com/nature).

**Acknowledgements** We thank M. Ratner, G. C. Schatz and R. van Duyne for discussions and advice. This work was supported by the Alfred P. Sloan Fellowship and the Dreyfus Teacher-Scholar Award (to B.A.G.).

**Author Contributions** H.N. performed the experiments, and collected and analysed the data; K.J.M.B., A.N., E.A.W. and B.A.G. developed the theoretical model; B.K. and R.K. synthesized nanoparticles and thiols; K.V.T. and M.M.A. helped with the construction of the Faraday cage and with data analysis; J.F.S. planned synthesis and helped with the interpretation of results; and B.A.G. conceived the experiments, analysed results, and wrote the paper.

**Author Information** Reprints and permissions information is available at [www.nature.com/reprints](http://www.nature.com/reprints). Correspondence and requests for materials should be addressed to B.A.G. ([grzybor@northwestern.edu](mailto:grzybor@northwestern.edu)).